[CANCER RESEARCH 64, 7302–7310, October 15, 2004]

Identification of Hypoxia-Regulated Proteins in Head and Neck Cancer by Proteomic and Tissue Array Profiling

Yijun Chen,[1] Gongyi Shi,[1] Wei Xia,[2] Christina Kong,[3] Shuchun Zhao,[3] Allison F. Gaw,[1] Eunice Y. Chen,[4] George P. Yang,[2] Amato J. Giaccia,[1] Quynh-Thu Le,[1] and Albert C. Koong[1]

[1]Department of Radiation Oncology, Center for Clinical Sciences Research, [2]Department of Surgery, Palo Alto VA Health Care System, Palo Alto, CA; [3]Department of Pathology, and [4]Department of Otolaryngology, Stanford University Medical Center, Stanford, California

ABSTRACT

Hypoxia within solid tumors decreases therapeutic efficacy, and identification of hypoxia markers may influence the choice of therapeutic modality. Here, we used a proteomic approach to identify hypoxia-regulated proteins and validated their use as endogenous indicators of tumor hypoxia. Using two-dimensional gel electrophoresis and PowerBlot (antibody-based array), we identified a group of 20 proteins that are increased ≥1.5-fold during hypoxia. The majority of these proteins such as IκB kinase β (IKKβ), MKK3b, highly expressed in cancer (HEC), density-regulated protein 1, P150^{glued}, nuclear transport factor 2, binder of ARL 2, Paxillin, and transcription termination factor I have not been previously reported to be hypoxia inducible. The increase in these proteins under hypoxia was mediated through posttranscriptional mechanisms. We additionally characterized the role of IKKβ, a regulator of the nuclear factor-κB transcription factor, during hypoxia. We demonstrated that IKKβ mediates cell survival during hypoxia and is induced in a variety of squamous cell carcinoma cell lines. Furthermore, we showed that IKKβ expression from tumor specimens correlated with tumor oxygenation in patients with head and neck squamous cell carcinomas. These data suggest that IKKβ is a novel endogenous marker of tumor hypoxia and may represent a new target for anticancer therapy.

INTRODUCTION

Hypoxia, a low oxygen environment within solid tumors, is a major determinant of local, regional, and distant failure after anticancer therapy (1–5). At the molecular level, hypoxia selects tumors with an increased malignant phenotype (6–9), resulting in resistance to apoptosis and greater propensity for distant metastases. Hypoxic cells are relatively resistant to conventional radiation and chemotherapy. In the absence of oxygen, a 3-fold increase in radiation dose is necessary to achieve the same level of tumor cell kill when compared with fully oxygenated conditions. Cells that are chronically hypoxic become quiescent but remain viable. They are capable of resuming cell growth during more favorable conditions. Most conventional chemotherapeutic agents target actively proliferating cells and thus are less effective in killing hypoxic cells. In addition, access of chemotherapy to the hypoxic regions of tumors can also limit the effectiveness in killing these cells (10, 11).

Our group and others have previously used cDNA microarrays to characterize global transcriptional changes that occur during hypoxia. These genes can be broadly categorized based upon their functions in metabolism, angiogenesis, invasion/tissue remodeling, apoptosis, and proliferation/differentiation (7, 12). Many of these genes contribute to tumor progression and increased malignancy. However, transcriptional changes alone are not sufficient to characterize the complexity of the tumor cell response to hypoxia. Other investigators have reported a poor correlation between mRNA and protein abundance (13, 14). Furthermore, a single gene can encode for more than one mRNA species through differential splicing, and proteins can undergo as many as 200 posttranslational modifications (15). These processes all contribute to a large number of different proteins that can be produced from a single gene. Interpretation of genomic and proteomic data are additionally complicated by the fact that we are only able to obtain a static picture of a highly complex, interrelated, and dynamic process.

Currently, there are many competing technologies and approaches to identify tumor hypoxia markers reliably for prognostic and therapeutic purposes (16). The aim of this study was to characterize global changes in the proteome during hypoxia to identify endogenous tumor markers of hypoxia. Using this approach, we have identified a group of hypoxia-regulated proteins that are induced by posttranscriptional mechanisms. These hypoxia-inducible proteins represent novel diagnostic/therapeutic targets. We also investigated the significance of one of these proteins, IκB kinase β (IKKβ), by correlating tumor oxygenation with expression of this protein in squamous cell carcinomas of the head and neck (HNSCC).

MATERIALS AND METHODS

Cell Culture, Hypoxia Treatment, and [^{35}S]Methionine Incorporation Assays. Human Fadu HNSCC cell lines were obtained from American Type Culture Collection (Manassas, VA). The IKKβ wild-type and knockout mouse embryonic fibroblasts were generously provided by Dr. Inder Verma (Salk Institute, San Diego, CA). All cells were cultured in DMEM supplemented with 10% fetal bovine serum. Desferrioxamine was used at a concentration of 100 μmol/L, and dimethyloxalyglycine was used at a concentration of 1 mmol/L. Cells were plated at 70 to 80% confluency and placed into a hypoxic chamber (Sheldon Manufacturing, Inc., Cornelius, OR) for the indicated duration. The chambers were gassed with a mixture of 95% nitrogen and 5% carbon dioxide, resulting in an oxygen level of <0.02%. For metabolic labeling, cells were cultured under hypoxic conditions for 2, 6, and 24 hours. At the indicated time, the cells were placed into serum-free DMEM without methionine/cysteine for 30 minutes and then labeled with complete media containing [^{35}S]methionine/cysteine (100 μCi/mL; Amersham Biosciences, Piscataway, NJ) for 30 minutes. All manipulations were performed in the hypoxia chamber with pre-equilibrated media to avoid any reoxygenation artifact. Cells were harvested and washed with PBS before lysis in buffer A (8 mol/L urea, 2% CHAPS). The solubilized proteins were precipitated with trichloroacetic acid and resolubilized in buffer. Total protein concentration was determined by the Bradford assay, a standardized spectrophotometric method to determine protein concentration based on light absorbance at 595 nm. We performed this assay according to the manufacturer's protocol (Bio-Rad, Hercules, CA).

Differential Centrifugation of a Two-Dimensional Gel Electrophoresis Sample. Two-dimensional gel electrophoresis sample preparation was performed by a differential centrifugation method as described by Hooper (17). Briefly, Fadu cells were lysed in two-dimensional gel electrophoresis sample buffer containing 8 mol/L urea, 2% CHAPS, 50 mmol/L DTT, and 0.2% Bio-Lyte 3/10 ampholytes. The crude cell homogenate was sonicated and centrifuged at 600 × *g* for 3 minutes. The supernatant was then centrifuged at

Received 3/12/04; revised 8/11/04; accepted 8/17/04.

Grant support: Stanford University Dean's Fellowship (Y. Chen), Stanford Cancer Council Research Award (C. Kong), American College of Surgeons Faculty Research Award (G. Yang), National Cancer Institute Grant CA67166 (Q-T. Le, A. Giaccia), and American Society of Therapeutic Radiology and Oncology Junior Faculty Research Award (A. Koong).

The costs of publication of this article were defrayed in part by the payment of page charges. This article must therefore be hereby marked *advertisement* in accordance with 18 U.S.C. Section 1734 solely to indicate this fact.

Requests for reprints: Albert C. Koong, Department of Radiation Oncology, Center for Clinical Sciences Research, Stanford University Medical Center, Stanford, CA 94305-5152. Phone: (650) 498-7703; Fax: (650) 723-7382; E-mail: akoong@stanford.edu.

6,000 × *g* for 8 minutes, the supernatant was again removed, and the final step was centrifuged at 40,000 × *g* for 30 minutes. The pellets from the first three steps were solubilized again in two-dimensional gel electrophoresis sample buffer.

Two-Dimensional Gel Electrophoresis and Mass Spectrometry Analysis. Eleven-centimeter immobilized pH gradient (IPG) strips with pH range 4 to 7 or 5 to 8 were rehydrated overnight in sample buffer containing equal amounts of total protein (300 to 450 μg). After isoelectric focusing using a protein isoelectric focusing apparatus (Bio-Rad), proteins were separated in the second dimension according to size. We used 4 to 20 or 10 to 20% gradient SDS-PAGE for 2 hours at 120 volts. All two-dimensional gels were run a minimum of three independent times under each condition to ensure reproducibility. Gels were stained with Sypro Ruby (Bio-Rad) and scanned with the Bio-Rad FX image system (Bio-Rad). The images were analyzed with PDQUEST 7.0.1 from Bio-Rad. Mass spectrometric analysis was carried out in the Proteomics Core Facility of the Southwest Environmental Health Sciences Center and Arizona Cancer Center. We attempted to identify proteins only from the bands that were consistently induced >2-fold across all of the gels. These proteins were excised and digested with trypsin or pepsin. Extracted peptides were analyzed by liquid chromatography-tandem mass spectrometry using a ThermoFinnigan LCQ Classic quadrupole ion trap mass spectrometer (San Jose, CA) equipped with a Michrom MAGIC2002 HPLC (Auburn, CA) and a nanospray ion source (University of Washington, Seattle, WA). Peptides were loaded onto 10-cm capillaries (365 × 100 μm inside diameter; packed with 5 to 6 cm of Vydac C18 material) that were pulled to 3- to 5-μm tips using a Sutter Instruments P2000 capillary puller (Novato, CA). Peptides were eluted at a flow rate of 200 to 300 nanoliter/minute into the mass spectrometer using reversed phase solvent conditions. Tandem mass spectrometry spectra data were analyzed with TurboSequest™[5] to assign peptide sequences to the spectra. TurboSequest analyses were performed against non redundant databases.

Immunoblotting. After treatment, cells were washed in PBS and lysed in buffer containing 9 mol/L urea, 15 mmol/L Tris-HCl, and 0.15 mol/L β-mercaptoethanol. Lysates were vortexed, sonicated, and centrifuged. For each sample, 50 μg of total protein were subjected to SDS-PAGE, transferred to nitrocellulose membrane, and immunoblotted with primary antibodies for 2 hours at room temperature. After washing, the membranes were probed with peroxidase-conjugated secondary antibodies at 1:3000 dilution for 1 hour. The bands were visualized using enhanced chemiluminescence reagents (Roche Diagnostics, Indianapolis, IN) according to the manufacturer's protocol. Sources of primary antibodies were as follows: cortactin (Upstate, Charlottesville, VA), heat shock protein 27 (HSP27; LabVision, Fremont, CA), and β-actin (Sigma, St. Louis, MO). All other antibodies used in this study were from BD Transduction Laboratories (Lexington, KY).

Real-time QPCR. Total RNA was obtained by lysing 5 to 10 × 10^6 cells directly in Trizol. Real-time QPCR was performed using an ABI PRIZM7900 machine (Applied Biosystems, Foster City, CA) and universal cycle conditions. Total RNA (1 μg) was reverse transcribed to cDNA, using random hexamer primers, per the manufacturer's recommendations (Applied Biosystems). A total of 1.5 μL of the synthesized cDNA served as substrate for PCR amplification of each gene of interest. Quantitative reverse transcription-PCR was performed in 384-well plates using specific primers and probes with the ABI PRISM 7900 Sequence Detection System. Each sample was assayed in triplicate. Results for PCR and reverse transcription-PCR experiments were analyzed using Sequence Detection Systems version 1.6.3 software. β-Actin was used to normalize mRNA concentration.

PowerBlot. After Fadu cells were exposed to hypoxia or maintained under aerobic conditions, protein extracts were additionally analyzed as follows. A total of 3 × 10 cm gradient gels was used to separate the protein, and 300 μg of protein were loaded onto each gel (10 μg/lane). The gels were run for 1.5 hours at 150 volts and then transferred to Immobilon-P membrane. The membranes were clamped with Western blotting manifolds capable of isolating 40 channels across each membrane. In each channel, a complex antibody mixture was added and allowed to hybridize for 1 hour at 37°C. The blots were removed from the manifold, washed, and hybridized for 30 minutes at 37°C with secondary goat antimouse antibody conjugated to Alexa680 fluorescent dye. The membranes were washed, dried, and scanned using the Odyssey IR Imaging System. The data from three independent runs were analyzed using a 3 × 3 matrix comparison method. We ranked the initial list of proteins based on their induction during hypoxia and the reproducibility of their induction in three independent hybridizations according to the manufacturer's guidelines.

After the initial analysis of the PowerBlot data, we modified the standard method provided by BD Biosciences Pharmingen (San Diego, CA) to better visualize low and high abundant proteins. We constructed three customized templates based on the signal intensity and quality from the first PowerBlot array. In the first set of customized templates, we used 13 antibodies with a strong signal intensity that originally saturated the signal on the initial array. For this template, we decreased the total protein loaded from 10 to 2 μg/lane. In the second set of customized templates, we used 39 antibodies that had a good but variable signal between the runs in the first array. We loaded the same amount of protein in this template. In the final set of customized templates, we used 63 antibodies that recognized proteins with a low expression on the initial array. For this group, we increased the total protein loading to 50 μg/lane. Each set of customized templates was run in triplicates.

Electromobility Shift Assays. Nuclear factor (NF)-κB activation was analyzed by electrophoretic mobility shift assay as described previously (18). Briefly, 10 μg of nuclear extracts were prepared from wild-type mouse embryonic fibroblast and IKKβ-knockout cells treated with normoxia and hypoxia. The extracts were incubated with ^{32}P end-labeled double-stranded NF-κB oligonucleotide (Promega, Madison, WI), and the DNA-protein complex was resolved on a 4% nondenaturing polyacrylamide gel. Protein binding to the NF-κB oligonucleotide resulted in slower migration of this complex, and these bands were visualized using a phosphorimager (Molecular Dynamics, Sunnyvale, CA). Specific binding was demonstrated by competing with unlabeled NF-κB oligonucleotide and by supershifting protein-DNA binding complexes with p50 antibody (Santa Cruz Biotechnology, Santa Cruz, CA). Competition with unlabeled mutant oligonucleotide had no effect on binding, and incubation with nonspecific antibody had no effect on supershifting protein-DNA complexes.

Patients. Patients with newly diagnosed HNSCC with accessible tumors were enrolled in two studies of tumor oxygenation approved by the Stanford Institutional Review Board (in accord with an assurance filed with and approved by the United States Department of Health and Human Services). A total of 101 patients participated in this study, of which, 6 did not have tumor oxygen measurements because of technical reasons. The patient and treatment characteristics of the patients initially evaluated for this study are included in Table 1. Of the remaining 95 patients, 7 patients had uninterpretable IKKβ staining (discordance between duplicate samples). Therefore, 88 patients with HNSCC were ultimately analyzed for this study.

Construction and Immunohistochemical Staining of Tissue Microarrays. The tissue microarray was constructed by taking representative 0.6-mm cores from 95 paraffin blocks of squamous cell carcinoma cases and by using

Table 1 *Patient and treatment characteristics*

Parameter	Criteria	No. of patients
Age	<60 y	55
(Median: 58)	≥60 y	46
Gender	Male	84
	Female	17
Site	Oropharynx	62
	Oral cavity	13
	Larynx	8
	Hypopharynx	12
	Others	6
T-stage	0–2	48
	3–4	53
N-stage	0–1	15
	2	66
	3	20
Stage	III	10
	IV	91
Hemoglobin	≤13	26
	>13	70
	Unknown	5
Median tumor pO_2	≤10 mm Hg	43
M(Median: 11 mm Hg)	> 10 mm Hg	52
	Inevaluable	6
Treatment	Chemoradiation	80
	Surgery +/− radiation	21

[5] Internet address: http://www.thermo.com/com/cda/product/detail/1,1055,16483,00.html.

a tissue arrayer (Beecher Instruments, Silver Spring, MD) to create a new paraffin block (19). Each individual core was confirmed to contain tumor by a trained pathologist before inclusion in the tissue array. In addition to the tumor samples, the microarrays also included control cores of skin, placenta, and benign lymph node. Each of the samples was present in the microarray as duplicate cores. Immunoperoxidase stains were performed on 4-μm thick sections of the tissue microarray. The slides were deparaffinized in xylene then dehydrated before antigen retrieval by microwaving in sodium citrate buffer (pH 6.0). The slides were then incubated with 10% normal horse serum followed by incubation with the primary antibody (1:1000 dilution IKKβ; Santa Cruz Biotechnology). After a PBS wash, the slides were incubated with the Vectastain Elite ABC kit and subsequently 3,3′-diaminobenzidine. The slides were coverslipped after a hematoxylin counterstain. The cores were interpreted by a pathologist and scored as follows: negative, 0; equivocal or uninterpretable, 1, weakly positive, 2; and strongly positive, 3.

Oxygen Tension Measurement. All measurements were performed using a computerized histograph (Sigma Eppendorf pO2 Histograph, Hamburg, Germany) as described previously (20). Fifty to eighty pO2 measurements in two to three tracks were recorded from each tumor, and an equal number of measurements was taken from normal subcutaneous tissues. Tumor pO2 was obtained from either the primary tumor or from the involved neck node. These measurements were pooled together based on previous data, indicating a highly significant correlation between pO2 measurements taken from the primary tumor or the involved neck nodes in the same patients for HNSCC (21). Computed tomography-guided placement of the electrode was used in patients with lymph nodes $\leq$ 2 cm. The measurements were presented in the form of histograms along with the calculation of a median pO2 and percentage of values $<$5 mm Hg (HF5 or hypoxic fraction $<$ 5 mm Hg) for each measured site. In all patients, the median tumor pO2 was consistently lower than that of normal subcutaneous tissues from the same patient.

Statistical Analysis. Statistical analysis was performed using Statview (SAS Institute, Inc., Cary, NC) statistical software. Because HF5 did not follow normal distribution, a Mann-Whitney rank test was used to compare HF5 values between the IKKβ-positive and -negative groups (22).

RESULTS

Hypoxia Inhibits Protein Synthesis. Upon exposure to hypoxia, protein synthesis in Fadu cells decreased rapidly as measured by [^{35}S]methionine incorporation. When compared with control cells, protein synthesis during hypoxia decreased to 74.9% (58.8 to 91.0%), 25.5% (18.6 to 32.4%), and 13.9% (10.2 to 17.6%) of the normoxic level after 2, 6, and 24 hours of hypoxia, respectively (Fig. 1*A*). The rapid decrease in protein synthesis was consistent with the results reported by others (23) and suggests that translational attenuation is an important early response to hypoxia. During these time points, we did not observe any significant change in the pH of the media ($<$0.4), nor was there any significant change in cell viability ($>$90% of cells were viable as assessed by trypan blue exclusion). We hypothesized that any proteins that were increased in this general background of decreased protein synthesis may be important mediators of the hypoxic stress response.

Identification of HSP27 and Cortactin by Two-Dimensional Gel Electrophoresis to be Elevated during Hypoxia. To determine global protein pattern changes during hypoxia, we used two-dimensional gel electrophoresis to separate hypoxia-regulated proteins. Using this method, we were able to resolve $>$1000 proteins from both normoxic and hypoxic samples (Fig. 1, *B* and *C*). We loaded an equal amount of total protein from cells cultured under hypoxic or aerobic conditions. Although *de novo* protein synthesis decreased during hypoxia (Fig. 1*A*), this change represents only a small fraction of the total

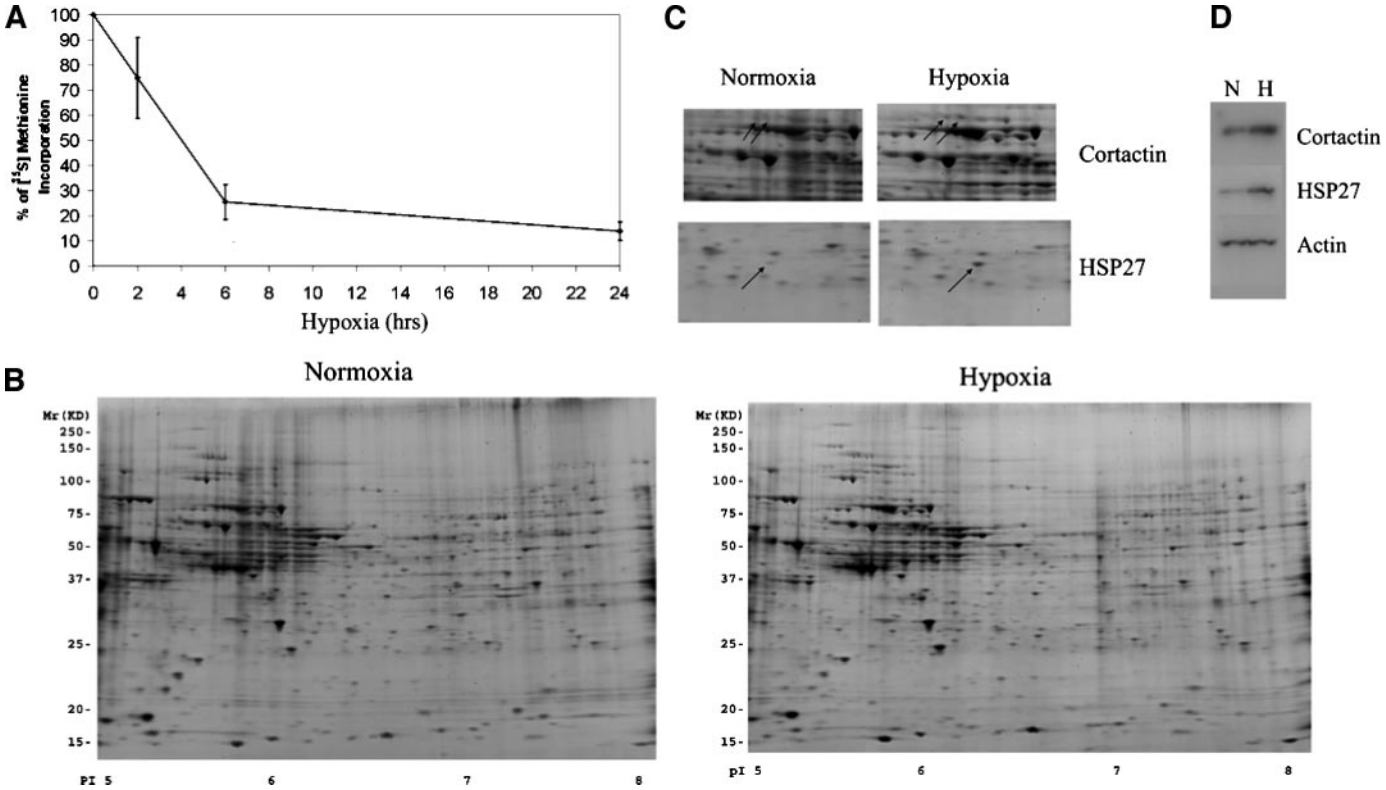

Fig. 1. *A.* ^{35}S-Metabolic labeling was used as a measure of protein synthesis during hypoxia in Fadu cells. After 2, 6, and 24 hours of hypoxia, protein synthesis decreases to 74.9, 25.5, and 13.9% of control cells. [^{35}S]Methionine incorporation was calculated as a percentage of incorporation during aerobic conditions. *B*, representative two-dimensional gels comparing global protein expression patterns in aerobic and hypoxic cells. In each of these gels, 300 μg of protein were loaded onto pH 5 to 8 strips. *C*, magnified view of two-dimensional gels with *arrows* highlighting the locations of cortactin and HSP27. Two isoforms of cortactin were resolved by this method. *D*. Western blot analysis of cortactin and HSP27 confirms their induction by hypoxia. Fifty micrograms of protein were loaded onto each lane. Cortactin antibody was diluted to a concentration of 1:2000, and HSP27 antibody was diluted to a concentration of 1:100. β-Actin was included as a loading control.

cellular protein. The majority of cellular proteins were not being actively synthesized, and therefore, the total cellular protein pool was not altered significantly. Furthermore, protein degradation was modestly decreased during hypoxia (data not shown), and these cells were growth arrested. The net effect on total cellular protein is complex, and loading an equal amount of total protein for two-dimensional gel electrophoresis analysis was a reasonable method of normalization. In all of our studies, the overall amount of cellular protein extracted did not differ by >30% between different experimental conditions. Using PDQuest software from Bio-Rad and a threshold of ≥2-fold, we found that >150 proteins decreased during hypoxia and <30 proteins increased during hypoxia. We chose to analyze proteins that were induced >2-fold because these proteins were most reliably induced when comparing changes across different two-dimensional gel electrophoresis experiments. The majority of the proteins did not change >2-fold when analyzed in this manner. We excised the protein spots that were most consistently increased during hypoxia and identified nine hypoxia-inducible proteins by liquid chromatography-tandem mass spectrometry. These proteins included dUTP pyrophosphatase, proteasome α type subunit, myosin light chain alkali, heterochromatin protein 1 γ, triosephosphate isomerase 1, thioredoxin-dependent peroxide reductase, cortactin, enolase, and HSP27. From this group, we confirmed by immunoblotting with commercially available antibodies that enolase (data not shown), HSP27, and cortactin protein levels were increased during hypoxia (Fig. 1*D*).

PowerBlot Antibody Array Revealed 17 Additional Proteins That Are Up-regulated during Hypoxia. We used another proteomic method to identify additional hypoxia-regulated proteins. Powerblot is an antibody-based Western array that can rapidly analyze the expression levels of >700 proteins (see Materials and Methods). Using the original PowerBlot Western array, we were able to detect 747 proteins and determined that 4 of these proteins were significantly increased during hypoxia (Fig. 2). These proteins included p53, cortactin, Jun, and neuronal pentraxin. However, because the original Western array was calibrated to detect a maximum number of proteins, lower abundance proteins were undetectable and higher abundance proteins gave saturating signals. Therefore, we designed several customized templates to optimize detection of these proteins. Using customized templates to group low (Fig. 3*A*) and highly expressed proteins (Fig. 3*B*) together, we were able to determine the expression level of those proteins with greater confidence. In the initial array, those proteins represented in Fig. 3*A* were barely detectable, and the proteins shown in Fig. 3*B* gave saturating signals. For example, in the original array, transcription termination factor I expression was at the limits of detection and induction during hypoxia could not reliably be assessed (Fig. 3*C*, top panel). In the subsequent customized array, we increased our detection sensitivity by loading more protein onto the gel and were able to determine the true induction pattern of transcription termination factor I (Fig. 3*C*, bottom panel). Conversely, in the original array, density-regulated protein 1 gave an oversaturating signal which prevented us from detecting its true expression (Fig. 3*D*, top panel). However, when less protein was loaded onto the customized array, we were able to detect induction of this protein (Fig. 3*D*, bottom panel). Thus, by varying the amount of protein loaded onto these custom arrays, we were able to identify additional hypoxia regulated proteins. Analysis of these custom arrays revealed that 14 additional proteins were increased during hypoxia [(Table 2, complete list of all proteins identified by Powerblot (18 proteins) and

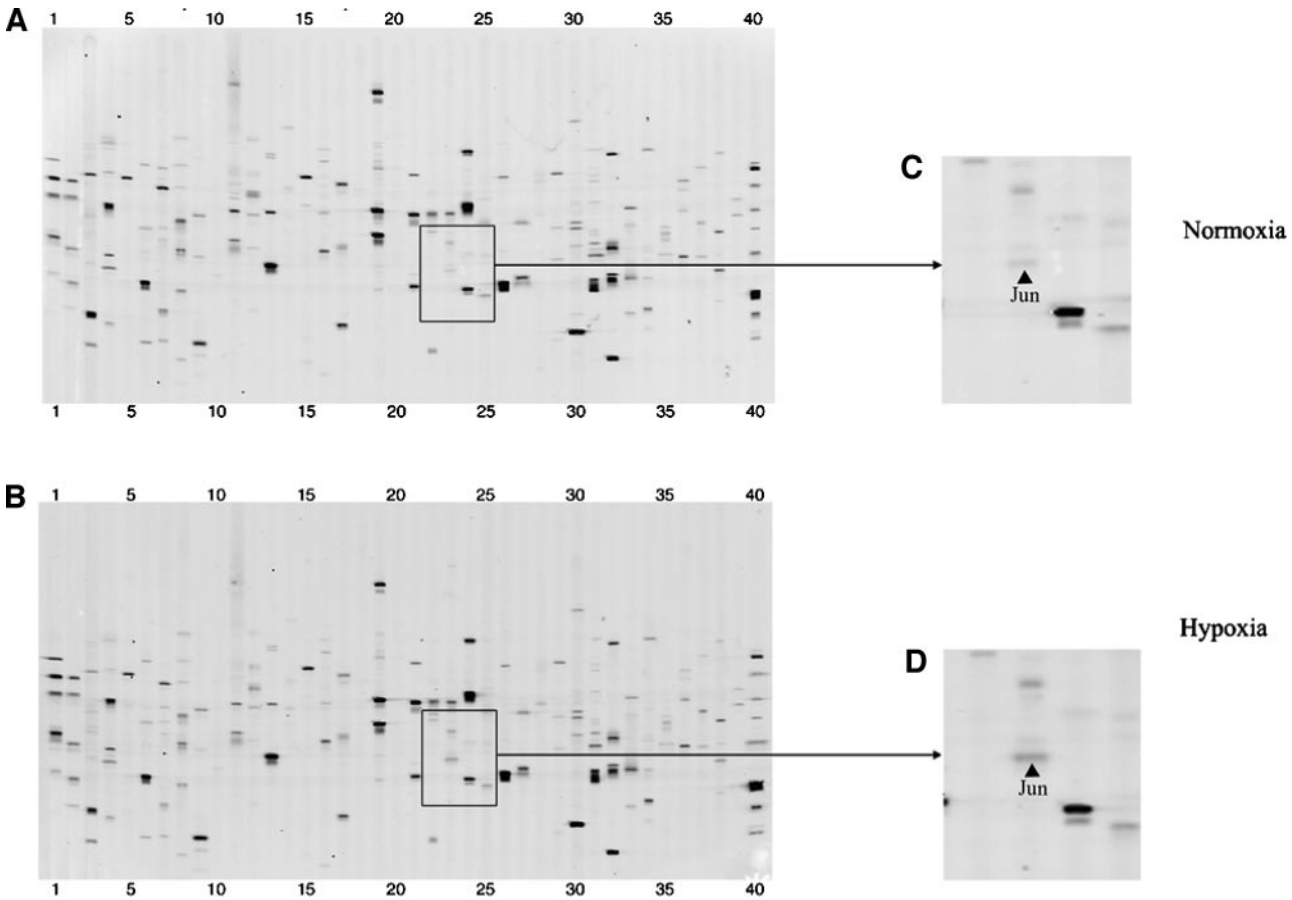

Fig. 2. PowerBlot analysis of protein expression in Fadu cells after a 24-hour exposure to hypoxia. One pair of representative templates from the original array is shown with *arrows* highlighting the location of Jun, a protein with increased expression during hypoxia. Each array was analyzed in triplicate.

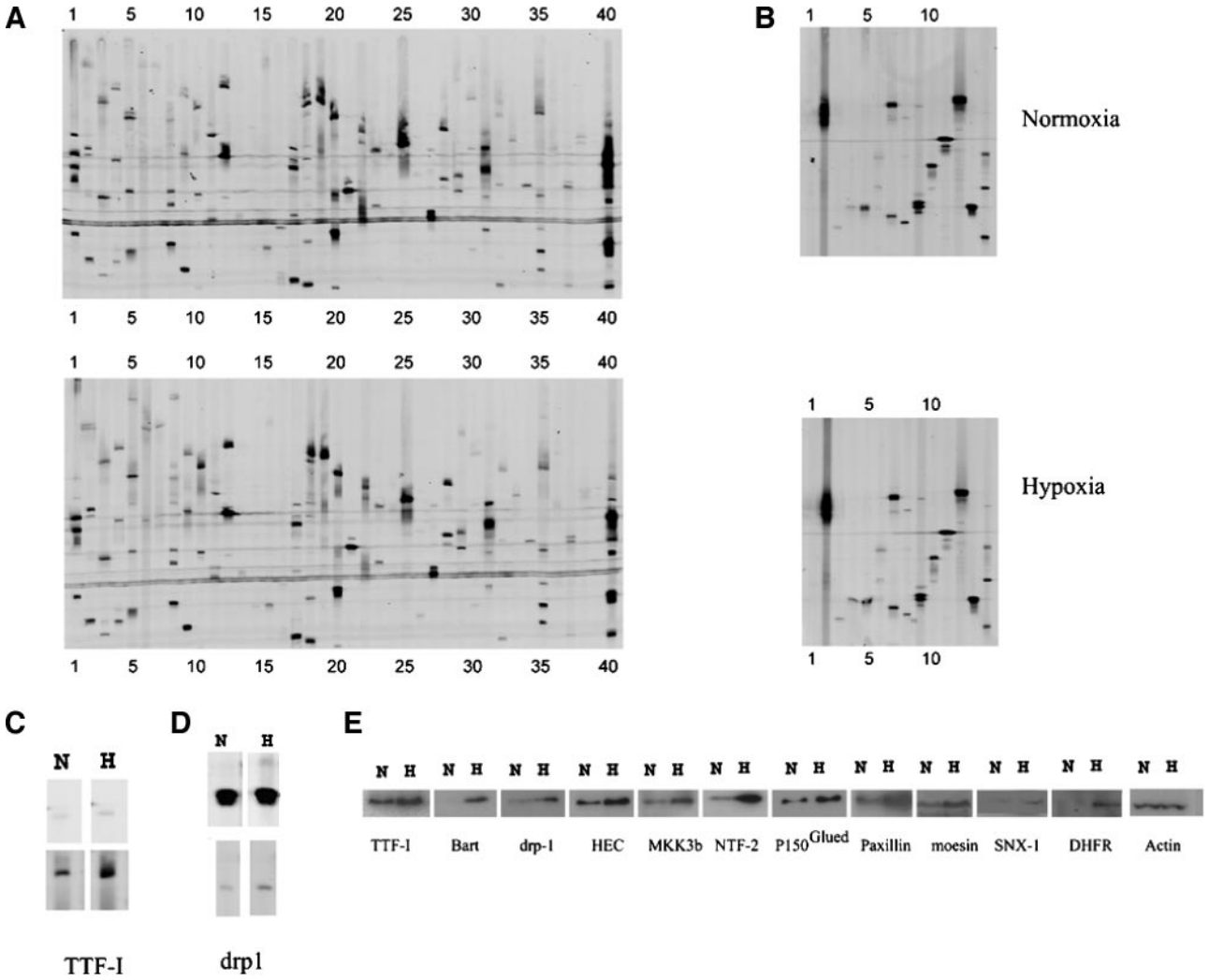

Fig. 3. *A*, customized array grouping together proteins with low expression on the original array. These proteins were barely detectable on the initial array. In these arrays, more protein (50 μg/lane) was loaded to maximize signal intensity. *B*, customized array grouping together proteins that gave saturating signals on the initial array. In these templates, less protein (2 μg/lane) was loaded to prevent saturation of signal. *C*, transcription termination factor I (TTF-I) expression in the original array is barely detectable (*top*) compared with its true expression pattern in the customized array (*bottom*). *D*, density-regulated protein 1 (drp-1) signal is saturated in the original array (*top*), which masks its induction as evident in the custom array (*bottom*). *E*, Western blotting of some of the hypoxia induced proteins that were identified by customized PowerBlot analysis. The dilutions of the primary antibodies were as follows: TTF-I (1:4000), binder of ARL 2 (Bart; 1:1000), drp1 (1:500), highly expressed in cancer (HEC; 1:250), MKK3b (1:100), nuclear transport factor 2 (NTF2; 1:1000), $P150^{glued}$ (1:250), Paxillin (1:1000), Moesin (1:400), SNX1 (1:150), and dihydrofolate reductase (DHFR; 1:150).

two-dimensional gel electrophoresis (three proteins, cortactin was found to be induced by both Powerblot and two-dimensional gel electrophoresis, the other two proteins were not present on the Powerblot array)]. A table detailing the reproducibility of these comparisons is included as supplementary data.

We performed Western blot analysis for each of these proteins to verify that their expression increased during hypoxia. We confirmed that the majority of these proteins were induced during hypoxia. Among these proteins, we identified some known hypoxia-inducible proteins (p53, p27, and HIF-1) and some novel hypoxia induced proteins (dihydrofolate reductase, highly expressed in cancer, IKKβ, density-regulated protein 1, $P150^{glued}$, nuclear transport factor 2, MKK3b, SNX1, binder of ARL 2, Paxillin, and transcription termination factor I; Fig. 3*E*).

Posttranscriptional Mechanisms for Hypoxic Induction. Table 2 is a compilation of all proteins that we identified to be induced by hypoxia either through two-dimensional gel electrophoresis or PowerBlot. To determine whether there was a transcriptional increase in these genes during hypoxia, we performed real-time QPCR after 24 hours of hypoxia for each of these genes. The results are listed in Table 2. There was no correlation between protein induction and mRNA induction among this group of genes, indicating that the increased levels of these proteins was not mediated by a transcriptional-dependent pathway. This observation suggests that posttranscriptional mechanisms affecting gene expression during hypoxia may be a significant factor influencing proteome changes. Furthermore, we analyzed the aerobic expression of several proteins (nuclear transport factor 2, paxillin, moesin, and HSP27) listed in Table 2 in the presence of proteosome inhibitors. These proteins demonstrated increased expression in the presence of proteosome inhibitors (data not shown), indicating that that protein degradation may play an important role in their regulation.

IKKβ Is Induced by Hypoxia through an Unknown Posttranscriptional Mechanism and Is Required for Cell Survival during Hypoxia. Because of its role in the regulation of apoptosis and tumor growth (24) and our previous work demonstrating that NF-κB was activated by hypoxia (25, 26), we decided to further investigate the regulation and significance of IKKβ, a critical regulator of NF-κB by hypoxia. In Fig. 4*A*, we showed that IKKβ protein accumulated rapidly during hypoxia. Furthermore, there was not a corresponding

Table 2 *Rank list of proteins with >1.5-fold increase during hypoxia along with the corresponding mRNA change*

Protein	Swiss Prot ID	mRNA induction	Function	Fold protein
MKK3b	P97293	-2.3	Response to stress; regulation of cell proliferation	>10*
HIF-1α	Q16665	-1.9	Transcription factor; protein binding	13.7
Dihydrofolate reductase	P00376	-4.3	dTMP biosynthesis; response to chemotherapy	10.6
Paxillin	P49024	-1.0	Adaptors; tyrosine kinase substrates	4.0
Binder of ARL 2	Q9Y2Y0	-2.2	Cytoskeleton, GTPases; GTPase regulators	3.4
Moesin	P26038	-1.2	Nitric oxide, mitochondria	3.2
SNX1	Q13596	1.2	Endosome to lysosome transport; endocytosis	2.9
Jun	P05627	4.0	Tyrosine kinases; cell cycle control	2.8
Transcription termination factor I	Q15361	-2.2	Nuclear transport	2.4
IKKβ	O14920	1.2	Activation of NF-κB pathway	2.2
Nuclear transport factor 2	P13662	-1.8	Nucleocytoplasmic transport; protein-nucleus import	2.2
P150^{glued}	P28023	-1.4	Axon cargo transport; neurogenesis; mitosis	2.2
p53	P13481	-1.2	Apoptosis; negative regulation of angiogenesis	2.2
Enolase	P06733	1.6	Glycolytic enzyme	2.0
Neuronal pentraxin	Q15818	-3.9	Cell adhesion; cytoskeleton	2.0
Kip1/p27	P46414	1.5	Regulation of cell cycle	1.9
HSP27	P04792	1.4	Response to oxidative stress	1.8
Density-regulated protein 1	O43583	-4.4	Cell communication; regulation of cell growth	1.8
Highly expressed in cancer	O14777	-2.1	G_2-M transition of mitotic cell cycle	1.7
Cortactin	Q14247	-1.3	Actin cytoskeleton organization and biogenesis	1.5

NOTE. The lack of correlation between protein and mRNA induction within these genes suggests hypoxia-regulated gene expression may be significantly influenced by posttranscriptional mechanisms.

* Exact fold induction unable to be determined because normoxic signal below threshold of detection.

increase in IKKβ mRNA (Fig. 4*B*), suggesting that this protein was regulated posttranscriptionally by hypoxia. We also examined the regulation of IKKβ in other squamous cell carcinoma cell lines (SCC4 and SCC25) and found that its induction was similar to Fadu cells (data not shown). To investigate the mechanism of IKKβ protein accumulation during hypoxia, we treated Fadu cells with two different prolyl hydroxylation inhibitors. Prolyl hydroxylation has been shown to mediate degradation of the hypoxia induced factor (HIF) family of transcription factors (27–29). As shown in Fig. 4*C*, dimethyloxalylglycine and desferrioxamine stabilized HIF-1α but had no effect on IKKβ stabilization. These results suggested that unlike HIF-1α protein stability, the mechanism of IKKβ protein induction was not related to inhibition of prolyl hydroxylation. To further investigate the role of HIF-1α, we also analyzed IKKβ expression in cells that were deficient in the von Hippel Lindau (VHL) tumor suppressor gene product. Cells that lack functional VHL have higher aerobic expression of HIF-1 and its downstream target genes. We did not observe any difference in basal IKKβ expression in cells with and without the presence of VHL. In contrast, basal HIF-1α expression was increased in cells that were deficient in VHL (data not shown).

By gel mobility shift assays (Fig. 4*D*), we showed that NF-κB activation by hypoxia and tumor necrosis factor α (TNF-α) was impaired in the absence of IKKβ. These studies, demonstrating that NF-κB activation is at least partially dependent upon IKKβ, were consistent with experiments reported by other investigators (30). The TNF-α–inducible complex was supershifted and the hypoxia-inducible complex was completely disrupted by the addition of p50 antibody. There was no effect on either supershifting or DNA binding when these extracts were incubated with a nonspecific antibody (data not shown). Overall, TNF-α activated NF-κB binding more strongly than hypoxia. Despite this limitation, however, the IKKβ-deficient cells definitely showed less binding under hypoxia than the wild-type cells. The decrease in NF-κB binding by hypoxia in the IKKβ-knockout cells also correlated with inhibition of cytoplasmic inhibitor of nuclear factor-κBα degradation and p65 nuclear accumulation (data not shown). These studies strongly support the role of IKKβ in the regulation of NF-κB activation by hypoxia and TNF-α. Other proteins within the IKK complex may also play a role because we did not observe complete inhibition of NF-κB activation by either hypoxia or TNF-α.

To determine the functional significance of IKKβ, we compared clonogenic survival after exposure to hypoxia in IKKβ wild-type and IKKβ-deficient mouse embryonic fibroblasts. The IKKβ-knockout cells were ~17-fold more sensitive to hypoxia compared with the wild-type mouse embryonic fibroblasts after exposure to 24 hours of hypoxia (Fig. 4*E*). These data suggest that IKKβ plays an important role in mediating cell survival during hypoxia.

IKKβ Tissue Expression Correlates with Hypoxia in Human HNSCC. To further validate the significance of IKKβ, we performed immunohistochemical studies using IKKβ-specific antibody in tissue sections of human HNSCC. We constructed a tissue array from 95 tumor samples in which we also recorded *in vivo* tumor pO2 measurements with the Eppendorf polargraphic microelectrode. Each tumor sample was arrayed in duplicate and scored blindly for staining intensity by a trained pathologist. A portion of this array is shown in Fig. 5*A*. Of the 95 cases, 7 were uninterpretable because of discordance between duplicate sections, 15 were negative, and 73 were positive. In Fig. 5*B*, representative examples of positive and negative staining are shown. Tumors with no IKKβ staining had a lower hypoxic fraction (HF5, fewer Eppendorf measurements < 5 mm Hg) than those with IKKβ staining. As shown in Fig. 5*C*, the difference between these two groups was statistically significant as determined by the Mann-Whitney rank test ($P = 0.001$) for nonnormal distributions.

DISCUSSION

In this report, we used two complementary proteomic approaches to identify novel hypoxia-regulated proteins. With the use of two-dimensional gel electrophoresis/tandem mass spectrometry and antibody-based arrays, we have identified a group of proteins that are induced during severe hypoxia in a posttranscriptional manner. Within human solid tumors, there is considerable heterogeneity with respect to measured oxygen levels with some tumors demonstrating a median pO2 of <5 mm Hg (31). Tumor cells are well adapted to survive for prolonged periods even during severe hypoxia, and our studies characterizing the tumor cell response to these levels of hypoxia are directly relevant to this subpopulation of cells.

Overall, our two-dimensional gel electrophoresis analysis revealed that the levels of most proteins were not increased under hypoxic compared with normoxic conditions. We hypothesized that any protein that was increased when translation was generally inhibited may play an important function in the adaptation to hypoxia and cell survival. Koumenis *et al.* (23) have also reported that protein synthe-

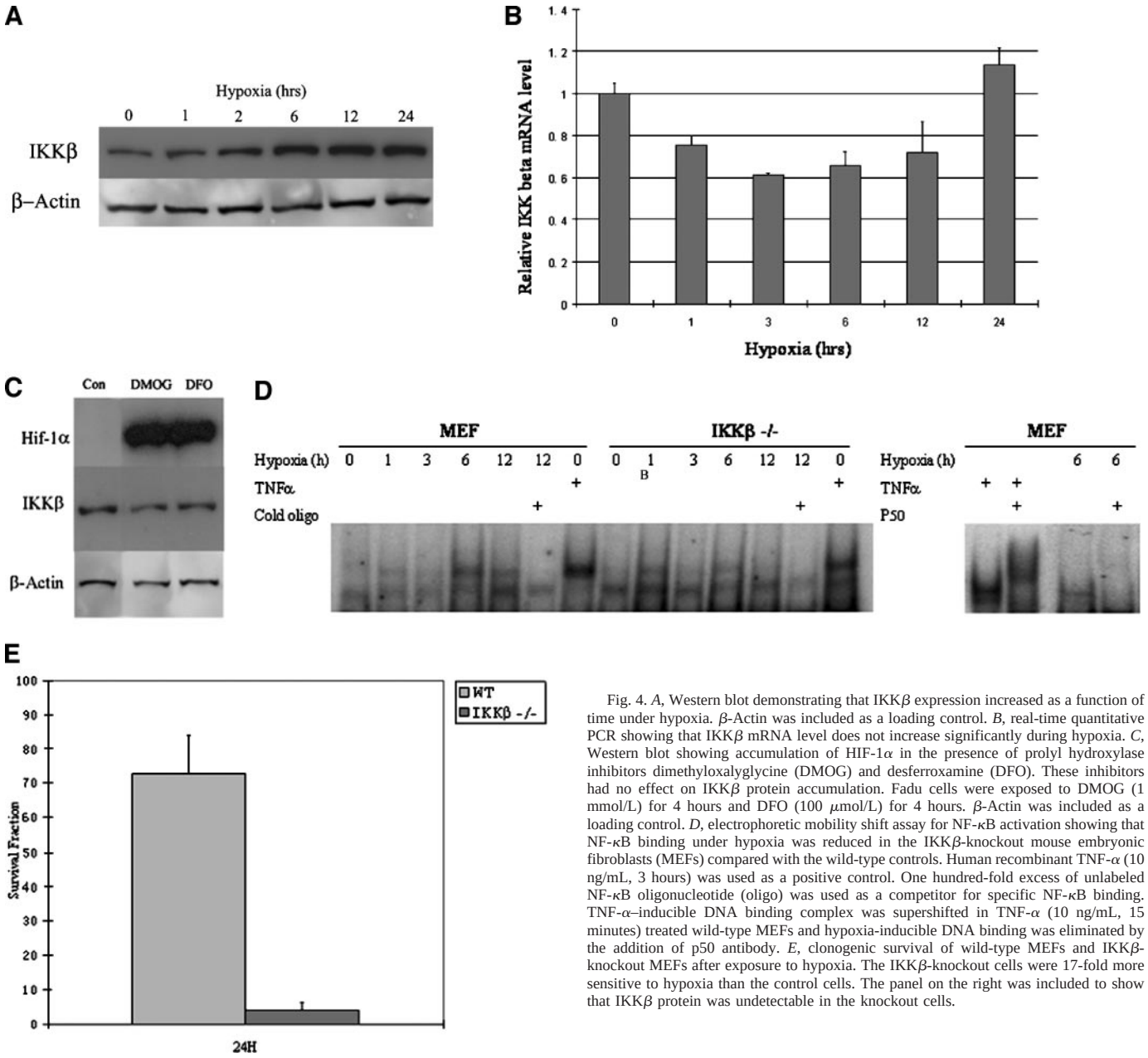

Fig. 4. *A*, Western blot demonstrating that IKKβ expression increased as a function of time under hypoxia. β-Actin was included as a loading control. *B*, real-time quantitative PCR showing that IKKβ mRNA level does not increase significantly during hypoxia. *C*, Western blot showing accumulation of HIF-1α in the presence of prolyl hydroxylase inhibitors dimethyloxalylglycine (DMOG) and desferroxamine (DFO). These inhibitors had no effect on IKKβ protein accumulation. Fadu cells were exposed to DMOG (1 mmol/L) for 4 hours and DFO (100 μmol/L) for 4 hours. β-Actin was included as a loading control. *D*, electrophoretic mobility shift assay for NF-κB activation showing that NF-κB binding under hypoxia was reduced in the IKKβ-knockout mouse embryonic fibroblasts (MEFs) compared with the wild-type controls. Human recombinant TNF-α (10 ng/mL, 3 hours) was used as a positive control. One hundred-fold excess of unlabeled NF-κB oligonucleotide (oligo) was used as a competitor for specific NF-κB binding. TNF-α–inducible DNA binding complex was supershifted in TNF-α (10 ng/mL, 15 minutes) treated wild-type MEFs and hypoxia-inducible DNA binding was eliminated by the addition of p50 antibody. *E*, clonogenic survival of wild-type MEFs and IKKβ-knockout MEFs after exposure to hypoxia. The IKKβ-knockout cells were 17-fold more sensitive to hypoxia than the control cells. The panel on the right was included to show that IKKβ protein was undetectable in the knockout cells.

sis decreased during hypoxia and that translational control during hypoxia was mediated by PKR-like endoplasmic reticulum kinase (PERK) phosphorylation of eIF2α. Furthermore, these investigators demonstrated that PKR-like endoplasmic reticulum kinase plays a role in mediating cell survival during hypoxia.

The relatively limited ability of two-dimensional gel electrophoresis to resolve and detect proteins reliably prevented the use of this technique as a comprehensive proteomic solution. Visualization of proteins by even the most sensitive methods requires ~1 to 10 ng, and reliable identification by liquid chromatography-tandem mass spectrometry requires that a similar amount be digested. All of the proteins that we identified by this method (HSP27, cortactin, and enolase) had relatively high levels of basal and inducible expression, which increased the likelihood of successful detection by two-dimensional gel electrophoresis and identification by liquid chromatography-tandem mass spectrometry. Therefore, two-dimensional gel electrophoresis was best used as a complementary technique to other proteomic methods. To identify other hypoxia-induced proteins, we used a modified Western array approach that allows detection of proteins in the picogram range. Using this method, we characterized the protein expression of >700 proteins with specific antibodies. From the 747 proteins detected, we found that 18 proteins were significantly increased by hypoxia. These proteins represented ~2 to 3% of all of the proteins included in the array, and the results were consistent with our [^{35}S]methionine incorporation experiments showing that protein synthesis decreased to <10% within 24 hours of hypoxia. Overall, within this group of 20 proteins (Table 2) identified by two different proteomic methods, we did not find any correlation between gene expression at the mRNA level with gene expression at the protein level. This suggested that during hypoxia, posttranscriptional mechanisms such as translational regulation, protein degradation, and protein stability may significantly influence protein expression. Therefore, a complete analysis of proteome changes during hypoxia should take into account transcriptional, as well as posttranscriptional regulation of gene expression.

Some of the hypoxia-regulated genes that we identified have been

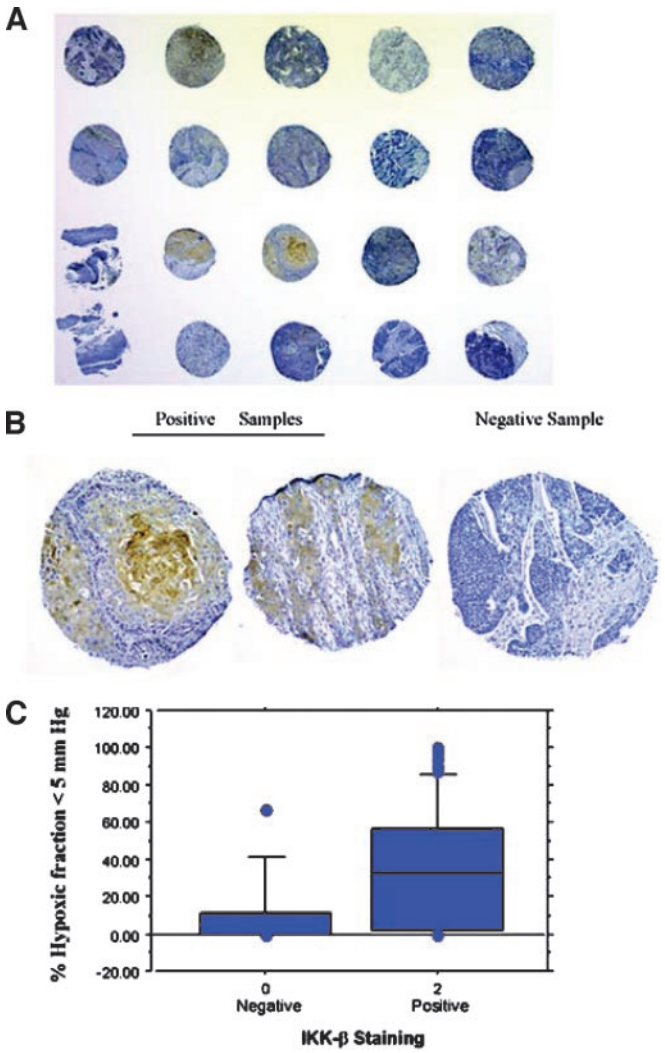

Fig. 5. *A*, a portion of the tissue array constructed from 95 tumor biopsy specimens from patients with squamous cell carcinomas of the head and neck. Each core biopsy specimen was arrayed in duplicate and scored by a trained pathologist who was blinded to the tumor oxygenation data. *B*, representative examples of IKKβ-positive and -negative staining from the tissue array. *C*. From each patient tumor represented on the array, we performed Eppendorf polargraphic microelectrode measurements of tumor oxygenation. We found a statistically significant correlation between tumor oxygenation and expression of IKKβ, suggesting that this protein may be a novel endogenous marker of tumor oxygenation.

previously reported to be elevated in squamous cell carcinomas. For example, cortactin amplification was detected in patients with HNSCC and correlated with advanced stage, poor histologic differentiation, recurrent disease, and reduced disease-specific survival (32). Another gene, highly expressed in cancer, was also amplified in squamous cell carcinomas of the esophagus (33) and postulated to be important in cell proliferation (34).

We chose to investigate in greater detail the role of IKKβ during hypoxia and to determine whether it may be used as an endogenous marker of tumor hypoxia in HNSCC. IKKβ was induced in several HNSCC cell lines at the protein but not at the mRNA level. Unlike HIF-1α protein stability, the mechanism of IKKβ protein stability was not related to prolyl hydroxylation because inhibitors of prolyl hydroxylation had no effect on IKKβ protein levels. Furthermore, there was no difference in IKKβ expression in cells with wild-type or mutant VHL. These results suggested that IKKβ protein expression is regulated by a mechanism distinct from HIF-1α.

Cells that were deficient in IKKβ were 17-fold more sensitive to hypoxia than wild-type cells after 24 hours of hypoxia. These studies indicated that IKKβ plays an important role in mediating survival during hypoxia. In IKKβ-deficient cells, NF-κB activation by hypoxia was significantly reduced, indicating that NF-κB activation is at least partially dependent upon IKKβ. These findings are consistent with the results reported for TNF-α–induced activation of NF-κB (30). We hypothesize that NF-κB activation triggers prosurvival signaling pathways and that inhibition of this pathway in the IKKβ-knockout cells contributes to the sensitivity of these cells to hypoxic stress.

Finally, we analyzed the expression of IKKβ in HNSCC tissue arrays derived from pretreatment tumor specimens in patients with Eppendorf measurements of tumor oxygenation. We found a strong correlation between IKKβ protein expression and tumor oxygenation, suggesting that it may be used as an endogenous marker of tumor hypoxia. The expression of IKKβ appeared to be specific to hypoxia because we did not find any correlation between expression of this protein and other prognostic factors such as tumor size, tumor site, stage, or degree of differentiation. In summary, we have found that IKKβ is induced by hypoxia and plays an important role in mediating cell survival under hypoxic stress. In human HNSCC, expression of this protein appeared to be a good indicator of tumor hypoxia and may represent a novel anticancer therapeutic target.

ACKNOWLEDGMENTS

We thank Erin Christofferson for excellent secretarial assistance, Jennifer Stevenson for suggestions regarding the PowerBlot assay, and members of the Koong, Le, and Giaccia lab for comments on the article.

REFERENCES

1. Brizel D, Prosnitz L, Scher R, Dewhirst M. Tumor hypoxia adversely affects the prognosis of carcinoma of the head and neck. Int J Radiat Oncol Biol Phys 1997;38: 285–9.
2. Brizel DM, Dodge RK, Clough RW, Dewhirst MW. Oxygenation of head and neck cancer: changes during radiotherapy and impact on treatment outcome. Radiother Oncol 1999;53:113–7.
3. Brizel D, Harrelson J, Layfield L, Bean J, Prosnitz L, Dewhirst M. Tumor oxygenation predicts for likelihood of distant metastasis in human soft tissue sarcoma. Cancer Res 1996;56:941–3.
4. Hockel M, Aral B, Mitze M, Schaffer U, Vaupel P. Association between tumor hypoxia and malignant progression in advanced cancer of the uterine cervix. Cancer Res 1996;56:4509–15.
5. Nordsmark M, Overgaard M, Overgaard J. Pretreatment oxygenation predicts radiation response in advanced squamous cell carcinoma of the head and neck. Radiother Oncol 1996;41:31–9.
6. Graeber T, Osmanian C, Jacks T, et al. Hypoxia-mediated selection of cells with diminished apoptotic potential in solid tumours. Nature (Lond.) 1996;379:88–91.
7. Koong AC, Denko NC, Hudson KM, et al. Candidate genes for the hypoxic tumor phenotype. Cancer Res 2000;60:883–7.
8. Young S, Hill R. Hypoxia induces DNA overreplication and enhances metastatic potential of murine tumor cells. Proc Natl Acad Sci USA 1988;85:9533–7.
9. Subarsky F, Hill R. The hypoxic tumor microenvironment and metastatic progression. Clin Exp Metastasis 2003;20:237–50.
10. Vaupel P, Kelleher D, Hockel M. Oxygen status of malignant tumors: pathogenesis of hypoxia and significance for tumor therapy. Semin Oncol 2001;28:29–35.
11. Brown J. Tumor microenvironment an the response to anticancer therapy. Cancer Biol Ther 2002;1:453–8.
12. Denko NC, Fontana LA, Hudson KM, et al. Investigating hypoxic tumor physiology through gene expression patterns. Oncogene 2003;22:5907–14.
13. Gygi SP, Rochon Y, Franza BR, Aebersold R. Correlation between protein and mRNA abundance in yeast. Mol Cell Biol 1999;19:1720–30.
14. Chen G, Gharib TG, Huang CC, et al. Discordant protein and mRNA expression in lung adenocarcinomas. Mol Cell Proteomics 2002;1:304–13.
15. Srinivas P, Srivastava S, Hanash S, Wright G. Proteomics in early detection of cancer. Clin Chem 2001;47:1901–11.
16. Evans SM, Koch CJ. Prognostic significance of tumor oxygenation in humans. Cancer Lett 2003;195:1–16.
17. Hooper N. Protein purification from animal tissue. In: RS, editor. Protein purification applications, 2 ed. Oxford University Press; 2001. p. 119–22.
18. Chaturvedi M, LaPushin R, Aggarwal B. Tumor necrosis factor and lymphotoxin: qualitative and quantitative differences in the mediation of early and late cellular response. J Biol Chem 1994;269:14575–83.
19. Liu CL, Prapong W, Natkunam Y, et al. Software tools for high-throughput analysis and archiving of immunohistochemistry staining data obtained with tissue microarrays. Am J Pathol 2002;161:1557–65.

20. Terris DJ, Dunphy E. Oxygen tension measurements of head and neck cancers. Arch Otolaryngol Head Neck Surg 1994;120:283–7.
21. Becker A, Hansgen G, Bloching M, Weigel C, Lautenschlager C, Dunst J. Oxygenation of squamous cell carcinoma of the head and neck: comparison of primary tumors, neck node metastases, and normal tissue. Int J Radiat Oncol Biol Phys 1998;42:35–41.
22. Glanz S, Slinker B. Primer of applied regression analysis of variance. New York: McGraw-Hill, Inc.; 1990. p. 50–109, 512–168.
23. Koumenis C, Naczki C, Koritzinsky M, et al. Regulation of protein synthesis by hypoxia via activation of the endoplasmic reticulum kinase PERK and phosphorylation of the translation initiation factor eIF2alpha. Mol Cell Biol 2002;22:7405–16.
24. Kucharczak J, Simmons MJ, Fan Y, Gelinas C. To be, or not to be: NF- kappaB is the answer—role of Rel/NF-kappaB in the regulation of apoptosis. Oncogene 2003;22:8961–82.
25. Koong AC, Chen EY, Giaccia AJ. Hypoxia causes the activation of nuclear factor kappa B through the phosphorylation of I kappa B alpha on tyrosine residues. Cancer Res 1994;54:1425–30.
26. Koong A, Chen E, Mivechi N, Denko N, Stambrook P, Giaccia A. Hypoxic activation of nuclear factor-kappa B is mediated by a Ras and Raf signaling pathway and does not involve MAP kinase (ERK 1 or ERK 2). Cancer Res 1994;54:5273–9.
27. Ivan M, Kondo K, Yang H, et al. HIF alpha targeted for VHL-mediated destruction by proline hydroxylation: implications for O2 sensing. Science (Wash. DC) 2001;292:464–8.
28. Jaakkola P, Mole DR, Tian YM, et al. Targeting of HIF-alpha to the von Hippel-Lindau ubiquitylation complex by O2-regulated prolyl hydroxylation. Science (Wash. DC) 2001;292:468–72.
29. Chan D, Sutphin PD, Denko NC, Giaccia AJ. Role of prolyl hydroxylation in oncogenically stabilized hypoxia-inducible factor-1alpha. J Biol Chem 2002;277:40112–7.
30. Li Q, Van Antwerp D, Mercurio F, Lee K, Verma I. Severe liver degeneration in mice lacking the IkappaB kinase 2 gene. Science (Wash. DC) 1999;284:321–5.
31. Brown J, Wilson W. Exploiting tumour hypoxia in cancer treatment. Nat Rev Cancer 2004;4:437–47.
32. Rodrigo JP, Garcia LA, Ramos S, Lazo PS, Suarez C. EMS1 gene amplification correlates with poor prognosis in squamous cell carcinomas of the head and neck. Clin Cancer Res 2000;6:3177–82.
33. Nakukuki K, Imoto I, Pimkhaokham A, et al. Novel targets for the 18p11.2 amplification frequently observed in esophageal squamous cell carcinomas. Carcinogenesis (Lond.) 2002;23:19–24.
34. Chen Y, Riley DJ, Chen PL, Lee WH. HEC, a novel nuclear protein rich in leucine heptad repeats specifically involved in mitosis. Mol Cell Biol 1997;17:6049–56.

Identification of Hypoxia-Regulated Proteins in Head and Neck Cancer by Proteomic and Tissue Array Profiling

Yijun Chen, Gongyi Shi, Wei Xia, et al.

Cancer Res 2004;64:7302-7310.